中國機械工程學刊第四十四卷第五期第 413~423 頁(民國一百一十二年)
Journal of the Chinese Society of Mechanical Engineers, Vol.44, No.5, pp413~423 (2023)

Improvement Design for A Double-Layer Honeycomb Structure using Uniform Design for Static and Dynamic Stress Analysis

Chi-Lung Tsai*, Chi-Chang Hsieh**and Yung-Chang Cheng**

Keywords：Double-layer honeycomb structure, von Mises stress, Deformation, ANSYS/LS-DYNA, Uniform design of experiment.

ABSTRACT

The objective of this article is to enhance the intensity of a double-layer honeycomb structure (HCS) under static forces and dynamic impact loads using the design of experiment method. A collection of simulation experiments is conducted using the uniform design (UD) method. The maximum von Mises stresses (VMS) in the honeycomb core (HCC) are calculated under ASTM tension and compression testing rules using static finite element analysis (FEA) through ANSYS/Workbench software. Dynamic FEA is employed to evaluate the maximum deformation of the HCS under the ASTM impact load testing simulation using ANSYS/LS-DYNA. In order to upgrade the energy absorption performance of the HCS, the maximum deformation of the HCC needs to be reduced under impact loads. Therefore, four objectives are considered simultaneously. The improved design of the double-layer HCS is obtained after executing the uniform design (UD). For the ASTM C297, C364, C365, and D7766 simulations, the improved design results in 15.4%, 29.78%, 3.29%, and 23.98% improvements over the original design, respectively. Subsequently, the UD technique creates a stronger double-layer HCC in the HCS.

Paper Received March, 2023. Revised May, 2023. Accepted July, 2023. Author for Correspondence: Yung-Chang Cheng

* *Graduate student: Ph. D. Program in Engineering Science and Technology, College of Engineering, National Kaohsiung University of Science and Technology, Taiwan 824, ROC.*

** *Professor, Department of Mechatronics Engineering, National Kaohsiung University of Science and Technology, Kaohsiung, Taiwan 824, ROC.*

*** *Graduate student: Department of Mechatronics Engineering, National Kaohsiung University of Science and Technology, Taiwan 824, ROC.*

INTRODUCTION

Honeycomb sandwich structures are utilized in various applications such as aircraft, railway vehicles, and race cars due to their favorable characteristics. The HCS can have diverse geometries, but all comprise an array of hollow cells enclosed by slim vertical walls. Typically, a single-layer sandwich structure comprises two metal plates and one honeycomb core. The strength of the sandwich panels is influenced by several factors such as the panel size, the facing material, and the density of the honeycomb cells in the panel.

A number of literatures (Aktay et al., 2008; Gao et al., 2020; Khan et al., 2020; Lu et al., 2015; Giglio et al., 2012) have performed static strength analyses on composite sandwich structures with honeycomb cores (HCCs). Aktay et al. (2008) determined the transverse crush performance of Nomex™ HCC materials. Gao et al. (2020) used experimental and numerical finite element analysis techniques to investigate the bending behavior of a HCS model. Khan et al. (2020) employed FEA to study the failure process for a hexagonal HCS made of Nomex™ polymer. Lu et al. (2015) investigated the three-point bending performance of a composite honeycomb sandwich plate using FEA. Giglio et al. (2012) performed flatwise compressive tests to develop an FEA model for a Nomex™ honeycomb core. The strength of the sandwich structures studied depended on various factors, such as the facing material, honeycomb cell density, and panel size.

Several studies have also employed dynamic stress analysis (Uğur et al. 2017; Li et al. 2014; Shen et al. 2013; Triplett and Schonberg 1998; Anderson and Madenci 2000). For instance, Uğur et al. (2017) applied the ASTM D7766 impact load testing standard to obtain FEA results for low-velocity impact testing of a HCS. Li et al. (2014) utilized LS-DYNA software to simulate an impact load and determine the optimal geometry dimensions for a HCS with a metal square core. Shen et al. (2013) employed ABAQUS software to determine the dynamic stress in a graded HCS, while Triplett and Schonberg (1998) used ABAQUS software for a

dynamic FEA of a circular honeycomb sandwich plate under a low-velocity impact. Additionally, Anderson and Madenci (2000) discussed the results of an experimental investigation concerning the low-velocity impact response of sandwich composites with the honeycomb structure.

Numerous papers have concentrated on optimizing the geometry of HCS systems (Paz et al. 2014; Gholami et al. 2016; Namvar and Vosoughi 2020; Qin et al. 2019; Ebrahimi and Vahdatazad 2015). Paz et al. (2014) increased the energy absorption capacity of a HCS by using Kriging interpolation and a multi-objective optimization algorithm. Gholami et al. (2016) presented the optimal design of a honeycomb core structure under uniformly distributed normal load using the particle swarm optimization method. Namvar and Vosoughi (2020) optimized the design of a hexagonal sandwich plate using particle swarm optimization and a genetic algorithm. Qin et al. (2019) used the graded thickness design approach to determine the ideal geometrical specifications of a hexagonal HCS with uniform thickness. Ebrahimi and Vahdatazad (2015) used a multi-objective particle swarm optimization algorithm to determine the maximum energy absorption capacity of a honeycomb sandwich cylindrical column.

Using static and dynamic FEA, numerous studies have identified the best configuration for a single-layer HCS. However, there have been no studies on the static and dynamic impact strength of a double-layer HCS using ANSYS/Workbench and ANSYS/LS-DYNA software, despite its use in F1 racing cars to increase driver safety. This study aims to investigate the effect of dynamic impact on a double-layer HCS, by determining its static and dynamic strength through FEA. Simulations are performed according to ASTM D7766, C297, C364, and C365 standards, using ANSYS/LS-DYNA and ANSYS/Workbench software to determine the maximum deformation and VMS for a HCC. A UD is used for a group of simulation experiments, and the results show an improvement in three VMSs and deformation compared to the original design. This study proposes a new UD that generates a stronger double-layer HCC in the HCS system, improving its overall design.

FINITE ELEMENT ANALYSIS FOR A HONEYCOMB STRUCTURE

Double Layer Honeycomb Structure Model

Aluminum HCS is widely utilized in engineering and vehicle applications for energy absorption and impact attenuation in race car design. In Figure 1(a) (Davies et al. 2012), the impact attenuator is positioned in front of the race car, and the HCS is used in this location to absorb the impact energy and decrease the car's weight. To achieve this goal, an aluminum HCS plate is utilized. This study employs an aluminum honeycomb structure with double-layer cores as an impact attenuator, as demonstrated in Figure 1(b).

This model incorporates two honeycomb cores made of aluminum alloy, surrounded by three stainless steel plates. The geometry of an HCS can take on many different shapes, but it is defined by a grid of empty cells encased by thin, vertical walls. This particular type of HCS finds application in railway transportation systems and race cars.

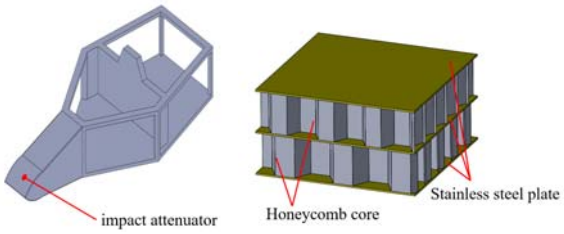

(a) (b)

Figure 1: (a) 3D model of a race car and (b) 3D model of a double layer honeycomb structure.

Standards for Testing Honeycomb Structure Models

In order to evaluate the strength of a double layer HCS, it is necessary to perform tensile, compression, and impact tests using the ASTM honeycomb structural standard, which must be verified by FEA. The tensile testing simulation according to the ASTM C297 standard (ASTM 2016) is depicted in Figure 2, where the test device is presented in Figure 2(a). In Figure 2(b), the double layer HCS is secured and held in place between rigid top and bottom mounts. The ends of the test piece are fastened to the testing apparatus through holes in the facing blocks. A load of 3000 N is applied to the rigid upper and lower mounts.

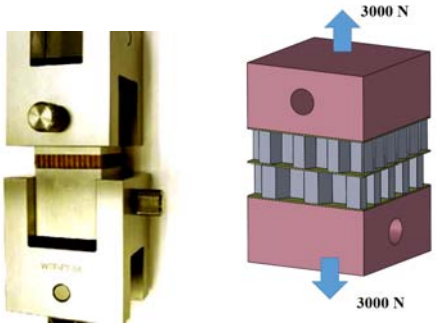

(a) (b)

Figure 2: (a) Investigational equipment and (b) arrangements for the ASTM C297 flatwise tensile test standard.

Figure 3 illustrates the simulation of the ASTM C364 compression test (ASTM 2016), where the compressive loads are applied parallel to the

specimen plates. Figure 3(a) displays the testing apparatus for the ASTM C364, where the force is applied to the double layer HCC through clamping or bonding supports. In Figure 3(b), the rigid upper and lower clamps are subjected to a compressive load of 3000 N.

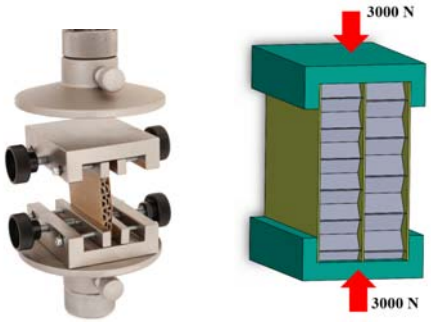

(a) (b)

Figure 3: (a) Investigational equipment and (b) arrangements for the ASTM C364 edgewise compressive test standard.

Figure 4 depicts the simulation of the ASTM C365 compression test (2016), where a uniaxial compressive force is applied perpendicular to the plane of the double layer HCS. The testing equipment is shown in Figure 4(a), where the loading plates attached to the testing device transmit the applied load to the HCC. The top and bottom stiff plates are subjected to a compressive load of 3000 N.

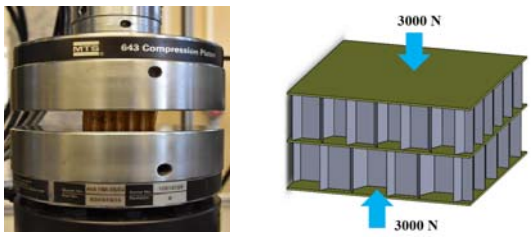

(a) (b)

Figure 4: (a) Investigational equipment and (b) arrangements for the ASTM C365 flatwise compressive test standard.

To evaluate the strength of a double layer HCS under impact loading, the HCC's ability to withstand damage is determined using dynamic FEA. Figure 5 provides the specifics of the ASTM D7766 damage resistance simulation for sandwich constructions (2016), where the experimental apparatus is displayed in Figure 5(a). During the ASTM D7766 test, a 6.35 kg hammer drops freely from a height of 205 mm above the HCS, as depicted in Figure 5(b), with the bottom of the HCS fixed in place.

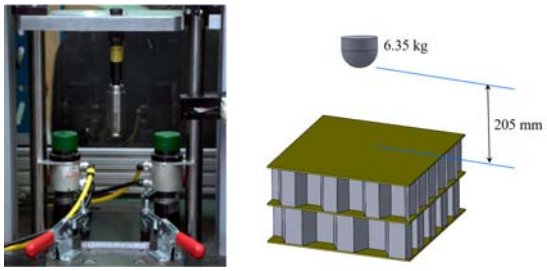

(a) (b)

Figure 5. (a) Investigational equipment and (b) settings for the ASTM D7766 damage resistance test for sandwich constructions.

Static FEA for Tensile and Compression Simulations

A double layer HCS is built as a 3D model using the SolidWorks software. The basically contact conditions and suitable material properties should be defined in the pre-processing for the FEA. Aluminum alloy 5052 is used for the HCC, and stainless steel is chosen for the plate, rigid mount, and the impactor. Table 1 displays the HCC and HCS's material characteristics that are pertinent to the static FEA. (ASM 2018a, 2018b) The meshing technique with the controlled element size is adopted in this paper. For the ASTM static loads testing simulations, the FEA uses element type C3D15 for the HCC.

Using ANSYS/Workbench software, the VMS layout in the HCC system are calculated. In accordance with ASTM C297, the mounted part is subjected to an exterior ductile load of 3000 N, as shown in Figure 6(a). The contact between each component is presumed to be bound. Mesh convergence analysis is for a HCC allows an accurate FEA. The HCC is meshed via the eligible finite elements for the ASTM C297 simulation. Figure 6(b) shows the convergent curving for the maximum VMS under the ASTM C297 testing simulation. The maximum VMS converges for an element size of less than 0.002 mm so 0.002 mm is used as the ideal elemental size. Figure 6(c) shows the maximum VMS layout under the ASTM C297 testing simulation for this element size, which is 3.14 MPa.

The HCC is meshed via the eligible finite elements for the ASTM C364 testing simulation. The mounted part is subjected to an exterior condensing load of 3000 N, in accordance with ASTM C364, as shown in Figure 7(a). Each part's contacts behave in a bonded manner. Figure 7(b) shows the convergent curving for the maximum VMS under the ASTM C364 testing simulation. 0.002 mm is the optimal elemental size because the maximum VMS converges for an element size of less than 0.002 mm. Figure 7(c) shows the maximum VMS layout under the ASTM C364 testing simulation for this element size, which is 6.17 MPa.

The HCS is meshed via the eligible finite elements for the ASTM C365 testing simulation. Figure 8(a)

shows that the plate is subjected to an exterior condensing load of 3000 N, in accordance with ASTM C365. The contact between each component is presumed to be bound. Figure 8(b) shows the convergent curving for the maximum VMS under the ASTM C365 testing simulation. The optimal elemental size is 0.002 mm because the maximum VMS converges for HCCs with elements smaller than 0.002 mm so. Figure 8(c) shows the maximum VMS layout under the ASTM C365 testing simulation for this element size, which is 112.65 MPa.

Table 1: Material properties for the HCS system

Part	Material	Property	Value
Honeycomb core	Aluminum Alloy (5052)	Young's Modulus(Pa)	6.9×10^{10}
		Poisson's Ratio	0.3
		Density (kg/m^3)	2700
		Yield strength (MPa)	193
Mount plate	Stainless Steel (AISI 304)	Young's Modulus (Pa)	1.93×10^{11}
		Poisson's Ratio	0.25
		Density (kg/m^3)	7860

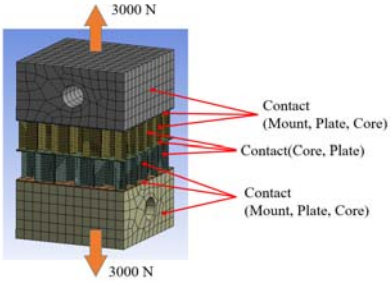

(a)

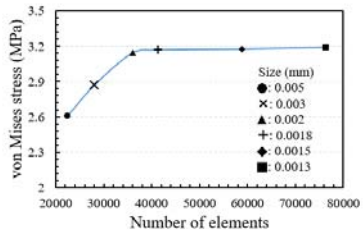

(b)

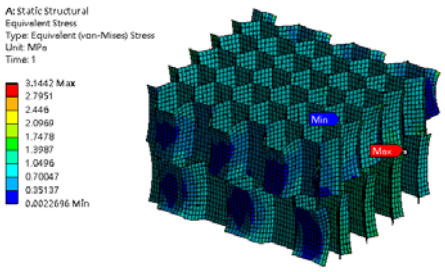

(c)

Figure 6: (a) Boundary conditions for the FEA model, (b) the convergence curve for maximum VMS and (c) the VMS layout for a HCC for the ASTM C297 tensile simulation.

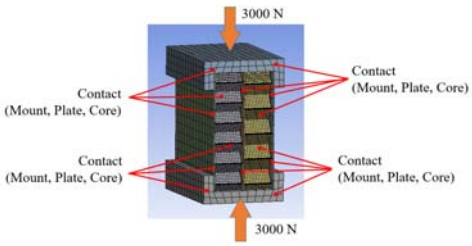

(a)

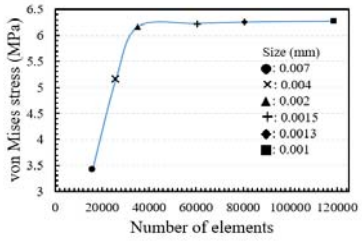

(b)

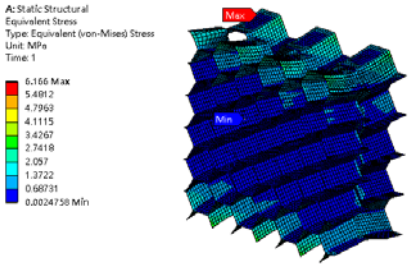

(c)

Figure 7: (a) Boundary conditions for the FEA model, (b) the convergence curve for maximum VMS and (c) the VMS layout for a HCC for the ASTM C364 compression simulation.

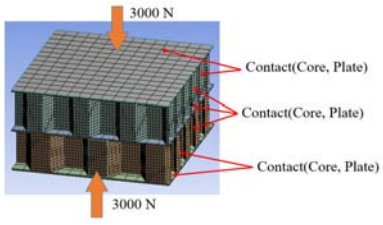

(a)

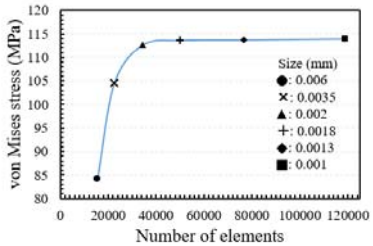

(b)

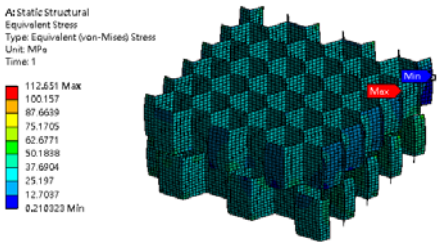

(c)

Figure 8. (a) Boundary conditions for the FEA model, (b) the convergence curve of maximum VMS and (c) the VMS layout for a HCC for the ASTM C365 compression simulation.

Dynamic Finite Element Analysis for Impact Simulation

In impact testing simulations, the crucial factor to consider is the HCC's deformation after the impact load has been applied to the HCS. As a result, minimizing the HCC's deformation is another objective function that needs to be improved. ANSYS/LS-DYNA software is utilized to assess the HCC's deformation. As per ASTM D7766, a 6.35 kg hammer is dropped from a height of 205 mm onto the HCS, resulting in an impact velocity of roughly 2.0 m/s, as shown in Figure 9(a). Additionally, the contact behavior of each component is considered to be confined.

The double layer HCC model is meshed using appropriate finite elements for the ASTM D7766 testing simulation. The convergent curve for the maximum deformation layout is presented in Figure 9(b). The maximum deformation converges when the element size is less than 0.003 mm, making 0.003 mm the optimal elemental size. The maximum deformation for this element size in the ASTM D7766 testing simulation is 9.99 mm, as shown in Figure 9(c).

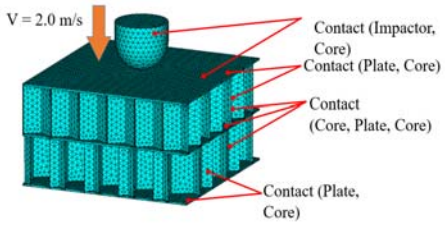

(a)

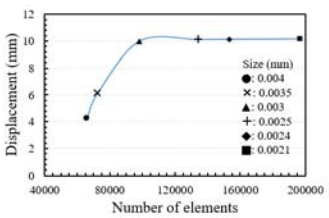

(b)

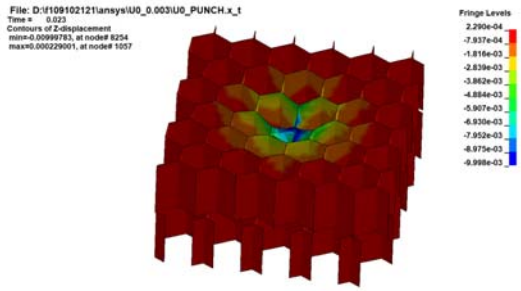

(c)

Figure 9: (a) Boundary conditions for the FEA model, (b) the maximum deformation convergence curve and (c) the deformation field for a honeycomb structure HCC for the ASTM D7766 damage resistance simulation for sandwich constructions.

IMPROVED DESIGN FOR A DOUBLE LAYER HONEYCOMB STRUCTURE

Factor Characteristic Analysis

The important and key control factors that need to be enhanced are the four double layer HCS parameters that have a major impact on the experimental indices. Figure 10 depicts the primary design parameters for the HCS. The stainless steel plate's thickness is indicated by the first control factor, TT. The second control factor, D1, means the diameter of the inside circle of the upper layer HCC. The diameter of the lower layer HCC's inscribed circle is represented by the third control factor, D2. The height of the lower layer HCC is determined by the fourth control factor, H. Table 2 lists the code numbers for each component as well as the upper and lower limits for each system control element.

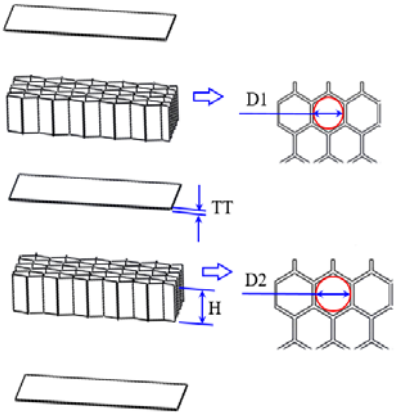

Figure 10. Control factors for the HCS model

Table 2. The lower and upper limits in HCS model

System control factor	Notation	Lower bound (mm)	Basic value (mm)	Upper bound (mm)
Thickness of the stainless steel plate	TT	0.9	1	1.1
Diameter of the inscribed circle of the upper layer honeycomb core	D1	15.3	17	18.7
Diameter of the inscribed circle of the lower layer honeycomb core	D2	18.9	21	23.1
Height of the lower layer honeycomb core	H	22.5	25	27.5

It is necessary to investigate the effects of the control factors on the objective functions such as von Mises stress and deformation. Although the influence of geometry dimensions on single-layer honeycomb structures has been discussed in some literature [Khan et al. 2020; Lu et al. 2015; Namvar et al. 2020], the impact of important geometry on the von Mises stress and deformation of double-layer honeycomb structures under ASTM C297, C364, C365, and D7766 testing simulations has not been discussed. Figures 11-14 present the influence of each control factor on the maximum von Mises stress (ST1, ST2, ST3) and deformation (DM) for the ASTM C297, C364, C365, and D7766 testing simulations, respectively.

In Figure 11(a), the influence of the thickness of the stainless steel plate (TT) on the maximum von Mises stress for the ASTM C297 and C364 testing simulations is illustrated. The maximum von Mises stress decreases and then increases as TT increases for the ASTM C297 testing simulation. Conversely, the maximum von Mises stress increases as TT increases for the ASTM C364 testing simulation. Figure 10(b) depicts the impact of TT on the maximum von Mises stress and deformation for the ASTM C365 and D7766 testing simulations, respectively. The maximum von Mises stress decreases as TT increases for the ASTM C365 testing. Additionally, the effect of TT on the maximum deformation of the honeycomb core decreases initially and then increases as TT increases for the ASTM D7766 testing.

In Figure 12(a), the effect of the diameter of the inscribed circle of the upper layer honeycomb core (D1) on the maximum von Mises stress for the ASTM C297 and C364 testing simulations is presented. The von Mises stress decreases smoothly as D1 is increased for the ASTM C297 testing. However, for the ASTM C364 testing simulation, the von Mises stress decreases initially and then increases as D1 is increased. In Figure 12(b), the influence of D1 on the maximum von Mises stress and deformation for the ASTM C365 and D7766 testing simulations, respectively, is shown. The von Mises stress decreases as D1 is increased for the ASTM C365 testing. Additionally, the maximum deformation of the honeycomb core increases initially and then decreases as D1 is increased for the ASTM D7766 testing simulation.

In Figure 13(a), the effect of the diameter of the inscribed circle of the lower layer honeycomb core (D2) on the maximum von Mises stress for the ASTM C297 and C364 testing simulations is investigated, respectively. The von Mises stress decreases as the D2 is increased for the ASTM C297 testing. Meanwhile, the von Mises stress decreases first and then increases as the D2 is increased for the ASTM C364 testing simulation. In Figure 13(b), the influence of D2 on the maximum von Mises stress and deformation for the ASTM C365 and D7766 testing simulations, respectively, is shown. The von Mises stress increases first and then decreases as the D2 is increased for the ASTM C365 testing. The deformation of the honeycomb core decreases first and then increases as the D2 is increased for the ASTM D7766 testing simulation.

In Figure 14(a), the influence of the height of the lower layer honeycomb core (H) on the maximum von Mises stress for the ASTM C297 and C364 testing simulations is shown. The von Mises stress hardly changes as H increases for the ASTM C297 testing, while it is decreased first and then increased as H is increased for the ASTM C364 testing simulation. In Figure 14(b), the effects of H on the maximum von Mises stress and deformation for the ASTM C365 and D7766 testing simulations are presented. The von Mises stress increases as H increases for the ASTM C365 testing. Additionally, the deformation of the honeycomb core decreases first and then increases as H increases for the ASTM D7766 testing simulation.

The influence of each control factor on the maximum von Mises stress of the honeycomb cores for the ASTM C365 testing simulation can be seen in Figures 11–14. This influence is more pronounced than that observed for the ASTM C297 and C364 testing simulations. Additionally, for the ASTM C297, C364, C365, and D7766 testing simulations, each control factor has a very substantial impact on the maximum deformation of the honeycomb cores.

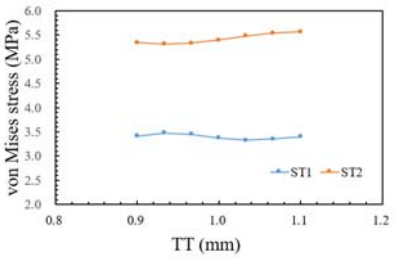

(a)

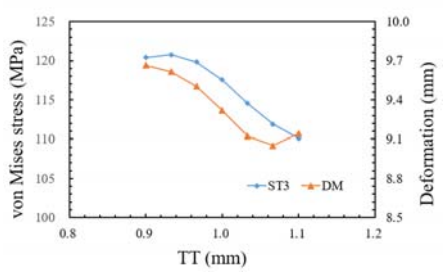

(b)

Figure 11: (a) The influence of the TT on the maximum von Mises stress for ASTM C294 and C364 testing simulations, (b) the influence of the TT on the maximum von Mises stress and deformation for ASTM C365 and D7766 testing simulations.

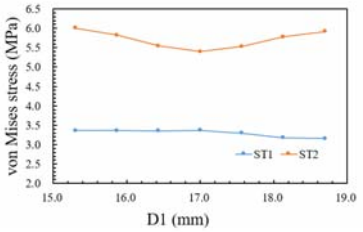

(a)

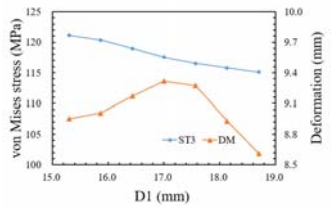

(b)

Figure 12: (a) The influence of the D1 on the maximum von Mises stress for ASTM C294 and C364 testing simulations, (b) the influence of the D1 on the maximum von Mises stress and deformation for ASTM C365 and D7766 testing simulations.

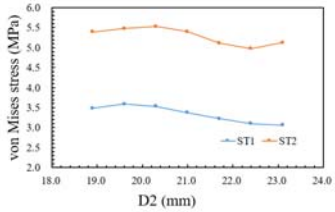

(a)

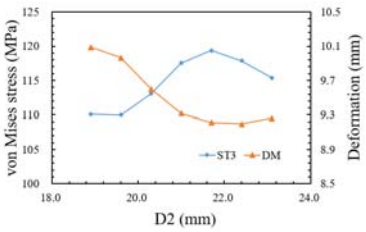

(b)

Figure 13. (a) The influence of the D2 on the maximum von Mises stress for ASTM C294 and C364 testing simulations, (b) the influence of the D2 on the maximum von Mises stress and deformation for ASTM C365 and D7766 testing simulations.

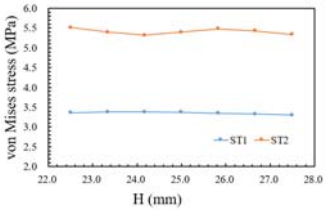

(a)

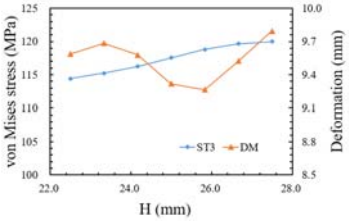

(b)

Figure 14. (a) The influence of the H on the maximum von Mises stress for ASTM C294 and C364 testing simulations, (b) the influence of the H on the maximum von Mises stress and deformation for ASTM C365 and D7766 testing simulations.

Uniform Design of Experiment

Due to the continuity of all control factors, the simulation experiments of the four control factors are arranged by the UD method. In a continuous design space, a series of experimental points are created using the UD. (Fang and Wang 1994) The continuous design space contains these experimental points that are uniformly distributed. This technique has been utilized in various technical and engineering fields. (Cheng and Wu, 2015; Lee et al. 2015; Song et al. 2016; Yudistiro et al. 2022)

The uniform table used in this study to generate the uniform experiments is $U_{16}^{*}\left(16^{12}\right)$. In this article, the UD table, $U_{16}^{*}\left(16^{12}\right)$, comprises 16 rows and 12 columns. It denotes that there are 12 control variables and 16 simulation experiments. Columns 1, 4, 5 and 6 of table $U_{16}^{*}\left(16^{12}\right)$ are used because there are only 4 control factors for the HCS. Each control factor has 16 equally spaced levels between its upper and lower boundaries. The values for the levels replace the number of levels. Table 3(a) shows all of the simulation experiments for $U_{16}^{*}\left(16^{12}\right)$. (Fang and Wang 1994)

The 3D geometric model is constructed using SolidWorks software for each simulation experiment's unique HCS design. ANSYS/Workbench and ANSYS/LS-DYNA are

employed to calculate the scattering of the VMS and deformation for the double layer HCC model, respectively. The maximum VMS and deformation for all experiments is calculated using FEA, as described in sections 2.3 and 2.4 and the results are listed in Table 3(a).

ST1 in Table 3(b) is the highest VMS in the HCC structure for the ASTM C297 tensile simulation. The highest VMS in the HCC structure for the ASTM C364 compression simulation is ST2. The maximum VMS in the HCC structure for the ASTM C365 compression simulation is ST3. DM sis the maximum deformation in the HCC structure for the ASTM D7766 impact simulation.

The highest VMS for the ASTM C297 tensile simulation decreases to 2.66 MPa in the third experiment following the application of the UD technique. In the third experiment, the maximum VMS under the ASTM C364 compression simulation drops to 4.33 MPa. Meanwhile, in the 15th experiment, the maximum VMS under the ASTM C365 compression simulation drops to 99.75 MPa. Moreover, the maximum deformation under the ATM D7766 impact simulation decreases 7.60 mm to in the 3rd experiment. Compared to the original design, Table 3(c) shows four positive improvements for ST1, ST2, ST3, and DM in the 3rd and 11th experiments. The improvement for each objective function is higher in the 3rd experiment than it is in the eleventh, though. As a result, the 3rd experiment's design is an improved design that makes use of the UD method. Figures 15 and 16 shows the results for the modified design.

Table 3. The simulation experiments and results for the uniform table $U_{16}^{*}\left(16^{12}\right)$

(a)

No.	TT (mm)	D1 (mm)	D2 (mm)	H (mm)
1	0.90	16.21	20.30	24.83
2	0.91	17.34	21.98	27.50
3	0.93	18.47	18.90	24.50
4	0.94	15.75	20.58	27.16
5	0.95	16.88	22.26	24.17
6	0.97	18.01	19.18	26.83
7	0.98	15.30	20.86	23.83
8	0.99	16.43	22.54	26.50
9	1.00	17.56	19.46	23.50
10	1.02	18.70	21.14	26.16
11	1.03	15.98	22.82	23.17
12	1.04	17.11	19.74	25.83
13	1.06	18.24	21.42	22.83
14	1.07	15.53	23.10	25.50
15	1.08	16.66	20.02	22.50
16	1.10	17.79	21.70	25.16

(b)

No.	ST1 (MPa)	ST2 (MPa)	ST3 (MPa)	DM (mm)
1	3.38	5.78	117.45	9.61
2	3.55	5.25	129.01	12.20
3	2.66	4.33	108.94	7.60
4	3.67	4.62	120.97	8.93
5	3.46	4.47	119.63	9.15
6	2.70	5.81	115.59	13.86
7	3.39	6.52	121.30	8.64
8	2.87	5.64	119.86	9.38
9	3.74	5.24	102.44	11.92
10	3.21	6.34	113.79	7.90
11	2.84	5.23	110.53	8.99
12	3.52	5.57	113.27	8.87
13	2.68	5.61	120.19	8.89
14	3.18	5.62	113.41	7.89
15	3.54	5.82	99.75	8.85
16	3.34	5.73	111.44	8.90

(c)

No.	Improvement in ST1 (%)	Improvement in ST2 (%)	Improvement in ST3 (%)	Improvement in DM (%)
1	-7.48	6.27	-4.25	3.86
2	-12.95	14.86	-14.52	-22.07
3	15.40	29.78	3.29	23.98
4	-16.78	25.01	-7.39	10.72
5	-9.89	27.49	-6.19	8.45
6	14.22	5.78	-2.60	-38.64
7	-7.89	-5.75	-7.67	13.62
8	8.81	8.57	-6.39	6.14
9	-18.96	15.01	9.06	-19.22
10	-1.95	-2.81	-1.01	20.92
11	9.66	15.21	1.89	10.03
12	-12.03	9.69	-0.55	11.27
13	14.84	9.05	-6.69	11.03
14	-1.17	8.83	-0.67	21.02
15	-12.67	5.66	11.45	11.43
16	-6.09	7.15	1.08	10.02

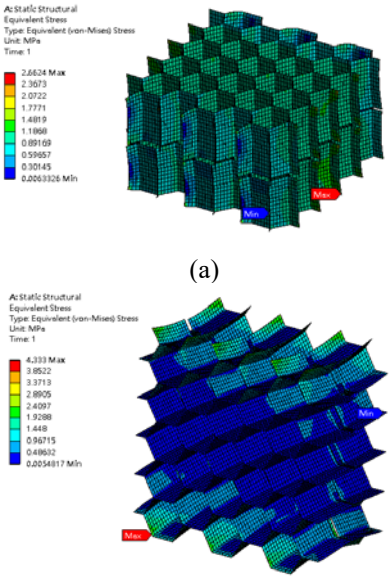

(a)

(b)

Figure 15: The distribution of the VMS for a double layer HCC using the improved design for (a) the ASTM C297 tensile simulation and (b) the ASTM C364 compression simulation.

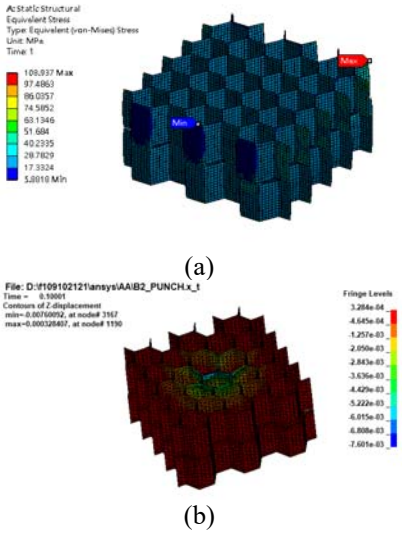

(a)

(b)

Figure 16: The distribution of VMS and deformation for a double layer HCC using the improved design for (a) the ASTM C365 compression simulation and (b) the ASTM D7766 impact simulation.

CONCLUSION

The strength of a double-layer HCS is determined using FEA. The HCS is subjected to static and dynamic loads according to ASTM testing standards, and a UD method is used to define the design space and conduct a number of simulation experiments. ANSYS/Workbench and ANSYS/LS-DYNA are used to determine the maximum VMS and deformation for a double-layer HCC under ASTM tension, compression, and impact load testing simulations, respectively. Before conducting the design of experiment, the characteristic analysis of each control factor has been investigated. According to the analysis's findings, each control component has a very significant influence on the maximum deformation of the honeycomb cores for the ASTM C297, C364, C365, and D7766 testing simulations. For ASTM standards C297, C364, and C365 simulations, the maximum VMS improvement using a UD method is 15.4%, 29.78%, and 3.29%, respectively. The improvement in maximum deformation is 23.98% for ASTM standard D7766 simulation. The use of UD reduces the maximum VMS in the HCC structure and decreases its deformation, allowing the HCC to absorb more energy. This study provides an improved design for a double-layer HCS.

ACKNOWLEDGEMENTS

The authors would like to express our gratitude and appreciation for the financial support of the Ministry of Science and Technology (MOST) under grant no's. 109-2221-E-992-022 and 111-2221-E-992-057. Furthermore, I would like to thank the undergraduate research team for their collaborative effort.

REFERENCES

Aktay, L., Johnson A. F. and Kroplin.B. H., "Numerical modelling of honeycomb core crush behavior," Engineering Fracture Mechanics, Vol. 75, No. 9, pp. 2616–30 (2008).

ASM Aerospace Specification Metals Inc. 2018a. AISI type 302 Stainless Steel. http://asm.matweb.com/search/SpecificMaterial.asp?bassnum=MQ302AC.

ASM Aerospace Specification Metals Inc. 2018b. Aluminum 5052-H38. http://asm.matweb.com/search/SpecificMaterial.asp?bassnum=MA5052H38.

ASTM International. 2016. ASTM C297/C297M: Standard Test Method for Flatwise Tensile Strength of Sandwich Constructions.

ASTM International. 2016. ASTM C364/C364M: Standard Test Method for Edgewise Compressive Strength of Sandwich Constructions.

ASTM International. 2016. ASTM C365/C365M: Standard Test Method for Flatwise Compressive Properties of Sandwich Cores.

ASTM International. 2016. ASTM D7766/D7766M-16: Standard Practice for Damage Resistance Testing of Sandwich Constructions.

Cheng Y. C. and Wu P. H., "Optimisation for suspension system of a railway vehicle with a new non-linear creep model developed by uniform design," International Journal of Heavy

Vehicle Systems, Vol. 22, No. 2, pp. 157-191 (2015).
Davies H. C., Bryant M., Hope M. and Meiller C., "Design, development, and manufacture of an aluminum honeycomb sandwich panel monocogue chassis for formula student competition," Proceedings of the Institution of Mechanical Engineers, Part D: Journal of Automobile Engineering, Vol. 226, No. 3, pp. 325-337 (2012).
Ebrahimi S., and Vahdatazad N., "Multiobjective optimization and sensitivity analysis of honeycomb sandwich cylindrical columns under axial crushing loads," Thin-Walled Structures, Vol. 88, pp. 90-104 (2015).
Fang K. T. and Wang Y., 1994. Number-Theoretic Methods in Statistics. London: Chapman & Hall.
Gao X., Zhang M., Huang Y., Sang L. and Hou W.,. "Experimental and numerical investigation of thermoplastic honeycomb sandwich structures under bending loading," Thin-Walled Structures, Vol. 155, pp. 106961-1~106961-14 (2020).
Gholami M., Alashti R. A. and Fathi A., "Optimal design of a honeycomb core composite sandwich panel using evolutionary optimization algorithms," Composite Structures, Vol. 139, pp. 254-262 (2016).
Giglio M., Gilioli A., and Manes A., "Numerical investigation of a three point bending test on sandwich panels with aluminum skins and Nomex™ honeycomb core," Computational Materials Science, Vol. 56, pp. 69–78 (2012).
Khan M. S., Abdul-Latif A., Koloor S. S. R., Petrů M. and Tamin M. N., "Representative cell analysis for damage-based failure model of polymer hexagonal honeycomb structure under the out-of-plane loadings." Polymers (Basel), Vol. 13, No. 1, pp. 52-1~52-23 (2020).
Lee C. K., Cheng Y. C. and Jiang C. P., "Explicit dynamic finite element analysis and uniform design with kriging interpolation and optimization to improve an on-road bicycle frame undergoing drop-mass impact test," Journal of the Chinese Society of Mechanical Engineers, Vol. 36, No. 4, pp. 353-361 (2015).
Lu C., Zhao M., Jie L., Wang J., Gao Y., Cui X. and Chen P., "Stress distribution on composite honeycomb sandwich structure suffered from bending load." Procedia Engineering, Vol. 99, pp. 405– 412 (2015).
Namvar A. R. and Vosoughi A. R., "Design optimization of moderately thick hexagonal honeycomb sandwich plate with modified multi-objective particle swarm optimization by genetic algorithm (MOPSOGA)," Composite Structures, Vol. 252, pp. 112626-1~112626-17 (2020).
Paz J., Díaz J., Romera L. and Costas M., "Crushing analysis and multi-objective crashworthiness optimization of GFRP honeycomb-filled energy absorption devices," Finite Elements in Analysis and Design, Vol. 91, pp. 30-39. (2014).
Qin R., Zhou J. and Chen B., "Crashworthiness design and multiobjective optimization for hexagon honeycomb structure with functionally graded thickness," Advances in Materials Science and Engineering, 2019, Article ID 8938696, pp. 1-13. (2019).
Shen C. J., Lu G. and Yu T. X., "Dynamic behavior of graded honeycombs – A finite element study," Composite Structures, Vol. 98, pp. 282-293. (2013).
Song G., Xu G., Quan Y., Yuan Q. and Davies P. A., "Uniform design for the optimization of Al2O3 nanofilms produced by electrophoretic deposition," Surface and Coatings Technology, Vol. 286, pp. 268-278 (2016).
Triplett M. H. and Schonberg W. P., "Static and dynamic finite element analysis of honeycomb sandwich structures," Structural Engineering and Mechanics, Vol. 6, No. 1, pp. 95-113 (1998).
Uğur L., Duzcukoglu H., Sahin O. S. and Akkuş H., "Investigation of impact force on aluminium honeycomb structures by finite element analysis," Journal of Sandwich Structures and Materials, Vol. 22, No. 1, pp. 87-103 (2020).
Anderson T. and Madenci E., "Experimental investigation of low-velocity impact characteristics of sandwich composites," Composite Structures, Vol. 50. pp. 239-247 (2000).
Yudistiro D., Cheng Y. C. and Jiang C. P., "Improved design for a two-piece dental implant system using fatigue and torsion testing simulation," Journal of the Chinese Society of Mechanical Engineers, Vol. 43, No. 5, pp. 463-471 (2022).

應用均勻設計於雙層蜂巢結構在靜動態分析下的改善設計

蔡騏隆, 謝其昌, 鄭永長
國立高雄科技大學 機電工程系

摘 要

本文的目的是利用實驗設計方法來提高雙層蜂巢結構（HCS）在靜態和動態衝擊載荷下的強度。使用均勻設計（UD）方法進行了一系列模擬實驗。使用 ANSYS/Workbench 軟體，根據 ASTM 拉伸和壓縮測試規則，蜂巢芯 (HCC) 中的最大von Mises等效應力 (VMS) 可由靜態有限元分析

(FEA) 計算得出的。使用 ANSYS/LS-DYNA動態有限元分析，計算 HCS 在的 ASTM 衝擊載荷測試模擬下的最大變形。為了提高HCS的能量吸收性能，需要降低HCC在衝擊載荷下的最大變形。因此，需要同時考慮四個改善的目標。執行均勻設計（UD）後得到雙層HCS的改善設計。對於 ASTM C297、C364、C365 和 D7766 模擬分析而言，改善的設計比原始設計分別提高了 15.4%、29.78%、3.29% 和 23.98%。由此可知，UD 技術在 HCS中有效地建立了更強的雙層HCC結構。